Aalborg Universitet

Aalborg University

DENMARK

An Improved Hybrid Prefiltered Open-Loop Algorithm for Three-Phase Grid
Synchronization

Verma, Anant Kumar; Jarial, Raj Kumar; Roncero-Sanchez, Pedro; Ungarala, Mohan Rao;
Guerrero, Josep M.

An Improved Hybrid Pre-Filtered Open-Loop Algorithm For Three-Phase Grid Synchronization

Anant K. Verma, *Member, IEEE,* R. K. Jarial, *Member, IEEE,* Pedro Roncero-Sánchez, *Senior Member, IEEE,* U. Mohan Rao, *Member, IEEE,* and Josep M. Guerrero, *Fellow, IEEE*

Abstract—In this article, a robust three-phase grid synchronization technique has been proposed for rapid detection of fundamental frequency, phase, and amplitude. The widely accepted phase locked-loop (PLL) algorithms possess complex architectures and require tedious tuning process for attaining a good stability margin. In order to surpass the shortfalls of PLL algorithms a computationally efficient, stable, and open-loop scheme has been reported in this work. A novel two consecutive samples based frequency estimator is developed for fast detection of the fundamental frequency. Moreover, an efficient hybrid pre-filtering approach is implemented based on the demodulation of the grid voltage signal. Additionally, the combination of a delayed signal cancellation operator and a band-pass filter allowed rapid rejection of DC-offset and harmonics, respectively. In the event of a grid voltage imbalance, the instantaneous symmetrical component (ISC) method is a rescuer for the rejection of the fundamental negative sequence (FNS) component without any delay. Subsequently, overall transient response time of the scheme is observed to be improved. On the other hand, the fundamental positive sequence (FPS) component facilitates the estimation of amplitude and phase angle information. Importantly, the dynamic performance of the proposed scheme has been experimentally validated in presence of various grid disturbances.

Index Terms—frequency estimation, grid voltage demodulation, moving average filter, three-phase system

I. INTRODUCTION

MICRO-GRIDS are mini utility grids deployed to support main power grid with increasing use of non-conventional energy sources to improve grid resilience [1].

Manuscript received November 05, 2019; revised January 27, 2020; accepted February 8, 2020.

A. K. Verma and R. K. Jarial are with the National Institute of Technology, Hamirpur 177005, India (e-mail: anant_verma12@ieee.org, jarial@nith.ac.in).

Pedro Roncero-Sánchez is with the Department of Electrical, Electronic, Control Engineering and Communications, Escuela Tecnica Superior de Ingenieros Industriales, Universidad de Castilla-La Mancha, 13071 Ciudad Real, Spain (e-mail: Pedro.Roncero@uclm.es)

U. Mohan Rao is with the Department of Applied Sciences University of Quebec at Chicoutimi Chicoutimi, QC G7H 2B1, Canada (e-mail: mohan.ungarala1@uqac.ca).

J. M. Guerrero is with the Center of Research on Microgrids (CROM) and was funded by a Villum Investigator grant (no. 25920) from the Villum Fonden, Department of Energy Technology, Aalborg University, 9220 Aalborg East, Denmark (Tel: +45 2037 8262; Fax: +45 9815 1411; e-mail: joz@et.aau.dk).

Typically, sophisticated power electronic converters [2] are often deployed in-order to ensure the function of active power distribution in the grid. Thus, fundamental frequency, phase, and amplitude information becomes key controllable parameters for the efficient functioning of grid-connected converters (GCCs) [3], [4]. Moreover, accurate and precise measurement of the frequency ensures continuous active power delivery to the grid via GCCs. For this purpose, a grid synchronization concept based control algorithm is essential to estimate the grid voltage parameters for the control, protection, and synchronization of GCCs [4]. The phase-locked loops (PLLs) [5], [6], frequency-locked loops (FLLs) [7], [8], enhanced-PLL (EPLL) [9], Kalman filter [10] are often exploitable algorithms for synchronization of single-phase and/or three-phase grid-tied inverters. Amongst these aforementioned approaches, PLLs and FLLs are the potential techniques for estimating fundamental grid voltage parameters. However, mutually related feedbacks are observable in these techniques which may affect the tuning process and the stability margin of the overall control scheme [11]. In a three-phase application, the versatility of PLLs and FLLs is due to simple control structure. Also, the grid attributes may be detected easily due to easy access to orthogonal signal generation (OSG), unlike the single-phase case [12]. Importantly, in the event of voltage imbalance, the major design challenge is to reject the fundamental negative sequence (FNS) component rapidly. The filtering schemes alone are incapable of rejecting the FNS component in the grid signal [13]. Thereby, a good solution is to apply the instantaneous symmetrical component (ISC) principle [14], which is successful with OSG-based pre-filtering methods. Moreover, the rapid extraction of the fundamental positive sequence (FPS) component is a widely accepted choice to implement a robust grid synchronization algorithm [15], [16]. Generally speaking, filters are universally preferred to obtain fundamental component from a harmonically distorted grid signal. Hence, the following filters are widely reported i.e. moving average filters (MAFs) [17], delayed signal cancellation (DSC) operators [18], all-pass filters [19], complex-coefficient complex-variable filter (CCVF) [20], demodulation based MAF-OSG [21], etc.

The demodulation [21]–[32] assisted filtering techniques are the subject of concern to the proposed work for demonstrating rapid rejection of FNS component, DC-offset, and harmonics. The demodulation schemes are sub-categorized into adaptive

and non-adaptive techniques, wherein filters are tuned to both off-nominal and nominal grid frequency, or nominal grid frequency alone. The non-adaptive demodulation schemes may lead to elevated phase errors [21]–[24] whereas, frequency adaptive approaches may avoid phase errors at the expense of an increase in the time response [25]–[27]. Moreover, another approach based on linear interpolation based finite impulse response (FIR)- low-pass filters (LPF) may suffer from phase and amplitude errors [28]. Herein, the pre-filtering stage is non-adaptive to the grid-frequency albeit the adaptability to grid-frequency is achieved through an error compensation approach. But, high-order FIR-LPFs may increase the computational complexity of the overall scheme. Importantly, non-adaptive schemes focus on open-loop frequency detection algorithms owing to small steady-state oscillations which might surpass the abilities of PLLs and FLLs. Feedback-less detection of the fundamental frequency is often made possible through digital signal processing (DSP) techniques [29]–[32]. As a matter of research investigation, the discrete oscillator law (DOL) is very appealing to estimate the frequency by storing three consecutive voltage samples of FPS component [30]. However, when the mid-sample value is zero, then DOL becomes numerically ill-conditioned [30], [31]. The removal of this ill-conditioning may be achieved by holding the past estimated frequency when the mid-sample tends to zero [30]. The spline modulating function based pre-filtering approach may eliminate the ill-condition through a recursive process which adheres to a trade off in response time and harmonic rejection ability of the scheme [31]. Thereby, an improved DOL (IDOL) technique [32] based on a MAF-OSG pre-filter may avoid recursion process by utilizing the quadratic sum of the mid samples of the orthogonal components (i.e. $v_\alpha(n-1)$ and $v_\beta(n-1)$) [32]. Therefore, the intent of this work is to address the key issues regarding a fast elimination of FNS, DC-offset, and harmonics using grid voltage demodulation. In addition, a new two-consecutive samples based open-loop frequency estimation algorithm is reported to improve the existing knowledge on the frequency estimation methods. The potential findings of this work are as follows:

1) An improved hybrid feedback-less filtering approach is proposed by incorporating DSC operator in series with a modified MAF-OSG structure.
2) The hybridization of filters allowed to modify the previously reported generic MAF-OSG structure (Fig. 1(a)).
3) The major benefits are an improved time response and

strong rejection of DC-offset and harmonics.
4) The ISC method assists in a fast extraction of the FPS component while rejecting the FNS component.
5) In frequency estimation, no numerical ill-condition and/or holding of previously estimated frequency is essential.
6) Under off-nominal frequency conditions, steady-state ripples in the estimated parameters are negligible.
7) An error compensation based on linear regression is deployed to obtain error-free estimated amplitude and phase information.

This article has been organized as follows: the hybrid pre-filtering stage requirements and extraction of FPS component are explained in Section II, the proposed frequency estimation technique is discussed in Section II, the amplitude and the phase angle estimation is presented in Section IV, the real-time simulation and experimental results been discussed in Section V. The article is summarized in Section VI.

II. Hybrid Pre-Filtering Stage (HPFS)

In practice, the fundamental grid voltage component is unavailable due to the distortion caused by non-linear loads connected to the grid. Undoubtedly, the actual grid signal will be contaminated with harmonics. In a three-phase grid signal, the negative sequence (NS) of nth harmonic produces distortions at $(n+2)$ and n^{th} harmonics [15]. Similarly, the NS of 5th harmonic will result in distortions of 5th and 7th harmonics. In a similar manner, the nth harmonic positive sequence sequence (PS) will result in a distortion of $(n-2)$ and n^{th} harmonics. For this reason, the 5th and the 7th harmonics in the grid voltage are consiered as dominant in this study[15], [16], whereas relatively smaller magnitudes of the 11th and the 13th harmonic components may be neglected.

A. Filtering Mechanism of HPFS

In this regard, a hybrid pre-filter solution is proposed which consists of a DSC operator (i.e. $DS_{0,7}$) cascaded with modified MAF-OSG (MM-OSG) structure, as shown in Fig. 1(b) which is collectively known as "HPFS". In general, the signal conditioning or measurement unit and several other reasons, such as half-wave rectification etc., may possibly inject a DC-offset in the grid signal. For this reason, a $DS_{0,7}$ is included in the pre-filtering stage which ensures a good rejection of the DC-offset and rejects the specific low-order harmonic (i.e. 7th harmonic) with minimum delay in the input signal. Further, the inclusion of the DSC operator also provides an insight to propose an

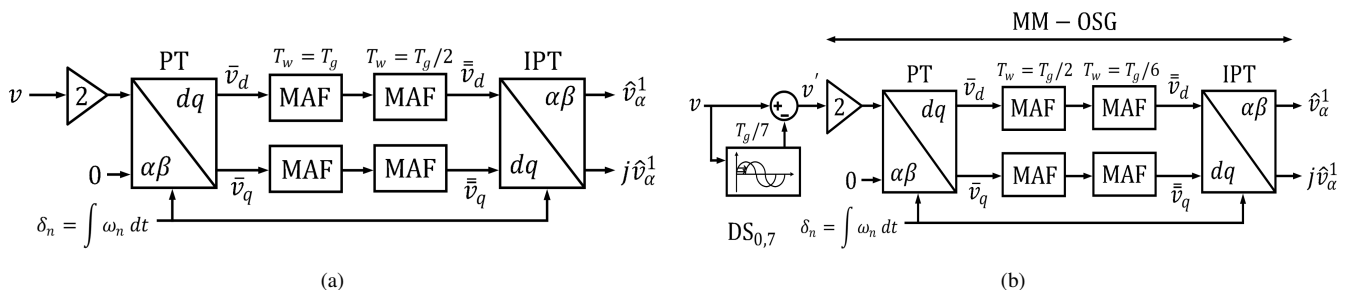(a)   (b)

Fig. 1. General structure (a) Generic MAF-based-OSG and (b) Proposed non-adaptive HPFS

improved version of the band-pass MAF-OSG (Fig. 1(a)) filter [24], [32] denoted as MM-OSG. For understanding purpose, a grid signal contaminated with a DC-offset, the 5th, and the 7th harmonic is expressed as shown below:

$$v(t) = A_1 sin(\omega_g t + \phi_1) + A_5 sin(5\omega_g t + \phi_5)$$
$$+ A_7 sin(7\omega_g t + \phi_7) + V_o \quad (1)$$

where, ω_g and V_o are the angular grid frequency and the DC-offset, respectively. The fundamental amplitude and the initial phase are denoted by A_1 and ϕ_1, respectively whereas amplitude and initial phase of the 5th and the7^{th} harmonic are denoted by A_5, A_7, and ϕ_5, ϕ_7, respectively. A delay of $\tau/7$ will be introduced in $v(t)$ for rejecting the DC-offset and the 7th harmonic as follows:

$$v' = \frac{v(t) - v(t - \tau/7)}{2} \quad (2)$$

where, $\tau = 2\pi/\omega_g$. Now, solving (2) and by utilizing the trigonometric identity as provided below:

$$sin(A) - sin(B) = \frac{1}{2}\left[cos(\frac{A+B}{2})sin(\frac{A-B}{2})\right] \quad (3)$$

The signal 'v'' is expressed as follows:

$$v' = A_1 sin(\frac{\omega_g\tau}{14}) sin(\omega_g t - (\frac{\omega_g\tau}{14} - \phi_1 - \pi/2))$$
$$+A_5 sin(\frac{5\omega_g\tau}{14}) sin(5\omega_g t - (\frac{5\omega_g\tau}{14} - \phi_5 - \pi/2))$$
$$v' = A_1 K_1 sin(\omega_g t - \Phi_1) + A_5 K_5 sin(5\omega_g t - \Phi_5) \quad (4)$$

where, $K_1 = sin(\frac{\omega_g\tau}{14})$, $K_5 = sin(\frac{5\omega_g\tau}{14})$, and Φ_1 is the net phase delay in the input signal. Therefore, only the fundamental amplitude and the phase will be affected, while the frequency information remains unaffected. Further, if ω_g is equal to nominal angular frequency ($\omega_n = 2\pi 50$ rad/s) then, the net delay offered by $DS_{0,7}$ to the input signal is approximately 0.143τ i.e. 2.86 ms. Using (4), the signal (v') free from DC-offset is then applied to a MM-OSG structure. In this strucure, the Park's transformation (PT) will perform the demodulation on v' by multiplying unit orthogonal components [21]–[27], tuned at $\delta_n(= \int \omega_n dt)$ to obtain the $dq-$frame components as follows:

$$\bar{v}_d = 2 v' cos(\delta_n) \quad (5)$$
$$\bar{v}_q = -2 v' sin(\delta_n) \quad (6)$$

Now, (5) is expanded as follows:

$$\bar{v}_d = A_1 K_1 sin((\omega_g + \omega_n)t - \Phi_1) +$$
$$+ A_1 K_1 sin((\omega_g - \omega_n)t - \Phi_1) +$$
$$A_5 K_5 sin((5\omega_g + \omega_n)t - \Phi_5) +$$
$$A_5 K_5 sin((5\omega_g - \omega_n)t - \Phi_5) \quad (7)$$

Similarly, (6) is expressed as follows:

$$\bar{v}_q = A_1 K_1 cos((\omega_g + \omega_n)t - \Phi_1) +$$
$$- A_1 K_1 cos((\omega_g - \omega_n)t - \Phi_1) +$$
$$A_5 K_5 cos((5\omega_g + \omega_n)t - \Phi_5) -$$
$$A_5 K_5 cos((5\omega_g - \omega_n)t - \Phi_5) \quad (8)$$

Subsituting, $\omega_g = \omega_n$ in (7) and (8), it may be observed that, the $dq-$frame components are only affected by double frequency component and even harmonics. Therefore, a MAF with a window length (T_w) equals to one-half of the fundamental period ($T_n/2$) is sufficient to reject even harmonics. However, under off-nominal frequency condition even harmonics will not be attenuated properly. To address this issue, a MAF with a $T_w = T_n/6$ is cascaded with a half-cycle MAF for improving the harmonic rejection capability. Later, the filtered $dq-$frame components [i.e. $\bar{\bar{v}}_d$ & $\bar{\bar{v}}_q$] are applied to the inverse PT tuned at ω_n for obtaining the fundamental orthogonal signals [$\hat{v}_\alpha^1(k)$ & $j\hat{v}_\alpha^1(k)$]. The delay (T_w) of HPFS is smaller than that of the standard MAF-OSG structure proposed in [32]. Thus, the improved transient response time (τ_d) of HPFS computed for a 50 Hz signal is,

$$\tau_d = 0.143\tau + T_n/2 + T_n/6 \approx 0.8096 \, cycle \quad (9)$$

For understanding the impact of $DSC_{0,7}$, the magnitude response plot of HPFS and the generic MAF-OSG is estimated using the AC frequency sweep method in a simulation environment, as shown in Fig. 2. It may be noted that the initial
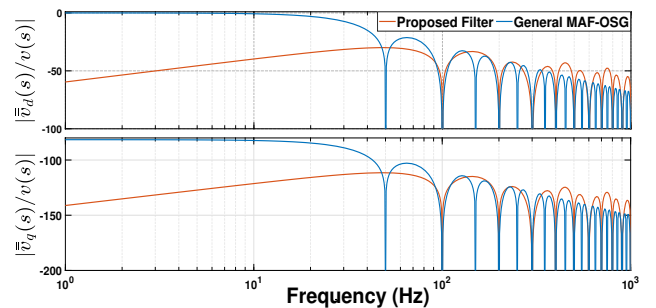
Fig. 2. Magnitude response plot for the $dq-$frame components with regard to the input signal

asymptote of the bode response plot does sufficiently rejects the DC-offset as compared to the MAF-OSG structure. In addition, the good elimination of the even harmonic components which are multiple of $2f_g$ is also possible. In the flowchart of the proposed scheme (Fig. 3), a simplified behavior of the scheme is presented, wherein a three-phase signal may be easily decomposed into stationary $\alpha\beta-$components through Clarke's transformation. Thereby, the v_α and the v_β components are then applied to two individual HPFS blocks to obtain the in-phase and the quadrature fundamental components which are utilized to extract the FPS components, i.e. $\hat{v}_\alpha^{1+}$ and $\hat{v}_\beta^{1+}$.

B. Extraction of the FPS components

The inclusion of HPFS block individually in the $\alpha\beta$-axes provide two-inphase ($\hat{v}_{\alpha\beta}^1$) and respective quadrature components ($j\hat{v}_{\alpha\beta}^1$) as depicted in Fig. 4. An instantaneous symmetrical component method [14] is then applied to the pairs of the fundamental orthogonal components to compute the FPS components without any delay. For simplicity, a relationship is developed as shown below:

$$\begin{bmatrix} \hat{v}_\alpha^{1+} \\ \hat{v}_\beta^{1+} \end{bmatrix} = \frac{1}{2} \begin{bmatrix} 1 & 1 \end{bmatrix} \begin{bmatrix} \hat{v}_\alpha^1 & j\hat{v}_\alpha^1 \\ -j\hat{v}_\beta^1 & \hat{v}_\beta^1 \end{bmatrix} \quad (10)$$
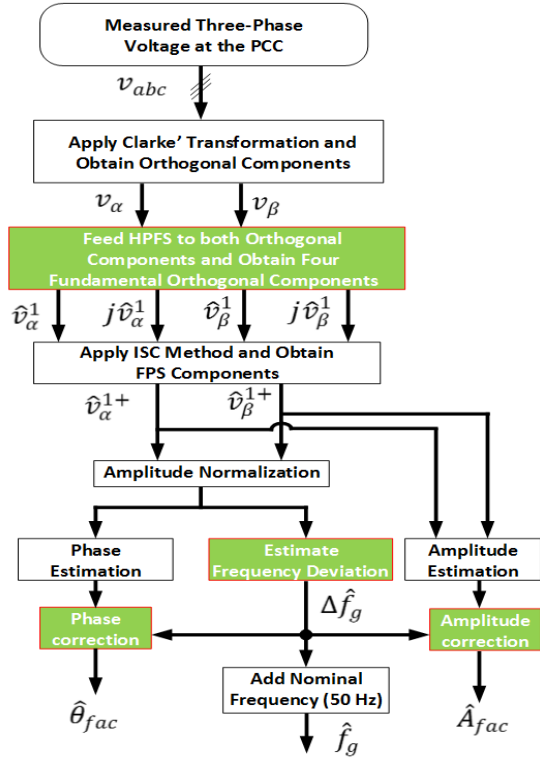
Fig. 3. Flowchart of the proposed scheme

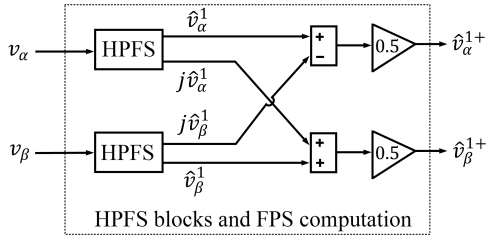The implementation details of (10) are provided in Fig. 4.

HPFS blocks and FPS computation

Fig. 4. Extraction of the FPS component

III. PROPOSED FREQUENCY ESTIMATOR

In this section, the implementation of the frequency estimation technique is discussed which is based on the storage of two consecutive samples of FPS components. For a real-time implementation, the discrete time FPS components are taken into consideration, as expressed below:

$$
\hat{v}_\alpha^{1+}(n) = A \sin (n \, \omega_g \, T_s + \theta)
$$
$$
\hat{v}_\beta^{1+}(n) = A \cos (n \, \omega_g \, T_s + \theta) \qquad (11)
$$

where, A, ω_g, θ, T_s, and n are the amplitude, the angular grid frequency, the phase angle, the sampling period, and the sampling instant, respectively. Herein, the normalized FPS components are utilized as given below:

$$
|\hat{v}_\alpha^{1+}(n)| = \frac{A}{\sqrt{(\hat{v}_\alpha^{1+})^2 + (\hat{v}_\beta^{1+})^2}} \sin (n \, \omega_g \, T_s + \phi)
$$

$$
|\hat{v}_\beta^{1+}(n)| = \frac{A}{\sqrt{(\hat{v}_\alpha^{1+})^2 + (\hat{v}_\beta^{1+})^2}} \cos (n \, \omega_g \, T_s + \phi) \qquad (12)
$$

The procedure regarding the generalized derivation of the algorithm by utilizing the voltage samples of unit $\alpha\beta$-components is provided below,

STEP-1: Product of voltage samples (PoVS):
For α-axis component, the product of two voltage samples is,

$$
M_1 = |\hat{v}_\alpha^{1+}(n)| * |\hat{v}_\alpha^{1+}(n - L)|
$$
$$
= sin^2(n\omega_g T_s) \, cos(L \, \omega_g T_s)
$$
$$
- sin(L \, \omega_g T_s) \, sin(n\omega_g T_s) \, cos(n\omega_g T_s) \quad (13)
$$

where, L is the distance between the samples i.e. $L = 1, 2,...$ N, $N \in I$. Similarly, for the β-axis component,

$$
M_2 = |\hat{v}_\beta^{1+}(n)| * |\hat{v}_\beta^{1+}(n - L)|
$$
$$
= cos^2(n\omega_g T_s) \, cos(L \, \omega_g T_s)
$$
$$
+ sin(L \, \omega_g T_s) \, sin(n\omega_g T_s) \, cos(n\omega_g T_s) \quad (14)
$$

STEP-2: Addition of PoVS and frequency estimation:
Add (13) to (14) yields:

$$
M_1 + M_2 = \underbrace{cos \, (L \, \omega_g T_s)}_{\text{DC-term}} \qquad (15)
$$

The estimated angular fundamental frequency is denoted by,

$$
\hat{\omega}_g = \frac{1}{L T_s} cos^{-1}(M_1 + M_2) \qquad (16)
$$

STEP-3: Estimation of deviation in frequency:
For small angular frequency deviation ($\Delta\omega_g$) from ω_n, then

$$
\omega_g = \omega_n + \Delta\omega_g \qquad (17)
$$

Substituting (17) in (15),

$$
\underbrace{cos(L \, (\omega_n + \Delta\omega_g) \, T_s)}_{\text{L.H.S}} = M_1 + M_2 \qquad (18)
$$

The expansion for *L.H.S* term is as follows:

$$
L.H.S = C_n \, cos(L \, \Delta\omega_g \, T_s) - S_n \, sin(L \, \Delta\omega_g \, T_s) \quad (19)
$$

where, $C_n = cos(L \, \omega_n T_s)$ and $S_n = sin(L \, \omega_n T_s)$. The frequency deviation (in Hz) is estimated as,

$$
\Delta \hat{f}_g = \frac{sin^{-1}}{L \, 2\pi \, T_s} \left[\frac{C_n \, cos(L \, \Delta\omega_g \, T_s) - (M_1 + M_2)}{S_n} \right] \quad (20)
$$

However, $\Delta\omega_g$ is unknown, thus equation (20) is made realizable by substituting $\Delta\omega_g(n-1)$ in place of $\Delta\omega_g$.

$$
\Delta \hat{f}_g = \frac{sin^{-1}}{L \, 2\pi \, T_s} \left[\frac{C_n \, cos(L \, \Delta\omega_g(n-1) \, T_s) - (M_1 + M_2)}{S_n} \right] \quad (21)
$$

Hence, the estimated frequency (in Hz) is,

$$
\hat{f}_g = f_n + \Delta \hat{f}_g \qquad (22)
$$

where, f_n is the nominal frequency (i.e. 50 Hz). Herein, L is the only calibration parameter which relies on the trade-off between the settling time (t_s) and steady-state accuracy. In a simulation environment, for $L = 30$, at t = 0.02 s, a step change of 2 Hz along with the harmonics ($h = 5, 7, 11, 13$) whose respective amplitude rounded up to a largest value computed through $v_h = 1/4h$ are considered in the grid signal, as shown
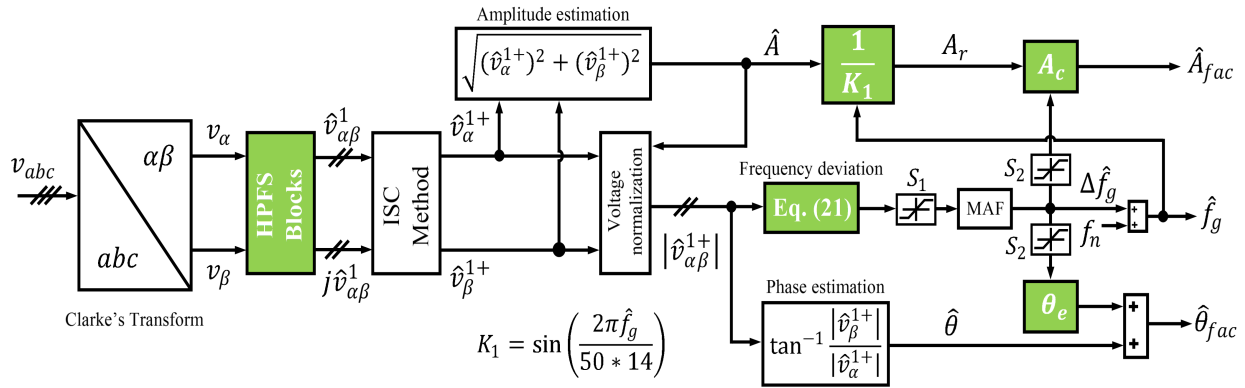
Fig. 5. Schematic diagram of the proposed scheme

in Fig. 6. The steady state ripple content in the estimated frequency is attenuated by including a half-cycle MAF in the path of the frequency estimation.

It is seen from the Table I that the proposed frequency estimator has attained good 't_s' and steady-state accuracy. It

TABLE I
SIMULATED DATA FOR SEVERAL *L*-VALUES

L	10	20	30	40	50
t_s (ms)	26	26.5	27	28	29
R. E. (%)	0.046	0.029	0.013	0.002	0.009

is to be noticed that, the relative error ($R.\ E.$) for $L \geq 30$ in the fundamental frequency estimation is well below 0.03% according to the IEC standard 61000-4-7 [34]. Moreover, the peak overshoot in Δf_g is forced to be limited in the range $-f_L - 1 + f_n$ and $f_U + 1 - f_n$ as per the EN50160 [33] standard, where the frequency range is 47 (f_L) – 52 (f_U) Hz with the help of the saturation block S_1 as depicted in Fig. 5. In addition, the saturation block S_2 helps in entire elimination of the transient overshoot in Δf_g which may reflect in amplitude and phase estimation with the lower and upper saturation limits as $(-f_L + f_n)$ and $(f_U - f_n)$. The overall schematic diagram of the proposed scheme is depicted in Fig. 5, wherein the colored blocks represent the important aspects of the proposed scheme.
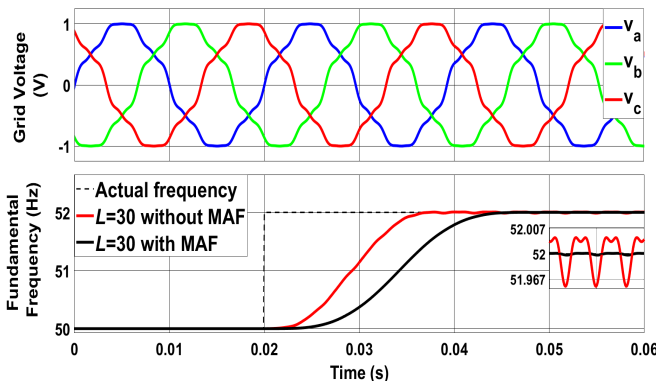

Fig. 6. Low-pass behaviour of the proposed frequency estimator

IV. ESTIMATION OF AMPLITUDE AND PHASE ANGLE

The grid side converters may be precisely controlled if the information on phase and amplitude is accurately available [4]. However, outputs of proposed HPFS will suffer loss in actual amplitude and the phase delay. The errors in amplitude and phase are dependent on the frequency deviation (Δf_g) [28]. Therefore, a mathematical relationship may be established as a function of Δf_g in order to compensate the errors and achieve grid frequency adaptability in an open-loop manner.

A. Amplitude estimation and error compensation

In the schematic shown in Fig. 5, the estimation of amplitude is computed as follows:

$$\hat{A} = \sqrt{(\hat{v}_\alpha^{1+})^2 + (\hat{v}_\beta^{1+})^2} \tag{23}$$

The loss in magnitude caused due to the DSC operator is recovered as follows:

$$A_r = \frac{\hat{A}}{K_1} = \frac{\sqrt{(\hat{v}_\alpha^{1+})^2 + (\hat{v}_\beta^{1+})^2}}{K_1} \tag{24}$$

where, $K_1 = sin(\hat{\omega}_g \tau / 14)$. Under off-nominal frequency condition, the actual amplitude of the FPS components is still erroneous owing to the MM-OSG filter. Thus, A_r will be treated as a reference and the errors in A_r are noted, as shown in Table II. Hence, a ratio of the actual amplitude

TABLE II
SIMULATED ERROR INFORMATION IN ESTIMATED AMPLITUDE AND PHASE

Δf_g (Hz)	-3	-2	-1	0	1	2
θ_e (rad.)	0.2977	0.3481	0.3985	0.4489	0.4993	0.5497
A_c	1.00167	1.00076	1.00023	1.00004	1.00022	1.00077
A_r	0.99833	0.99924	0.99978	0.99996	0.99978	0.99923

($A_{act} = 100\ V$) to A_r is then computed for six individual step changes (i.e. from 47-52 Hz) in the supply frequency, which is expressed as

$$A_c = \frac{A_{act}}{A_r} \tag{25}$$

Using (21), a curve fitting approach may be applied as shown in (26) to obtain the amplitude correction factor (A_c) as,

$$A_c = 0.0002 \left(\Delta f_g\right)^2 + 0.000002 \left(\Delta f_g\right) + 1 \quad (26)$$

where, the coefficients are generated from the parabolic curve shown in Fig. 7. The estimate of the actual fundamental
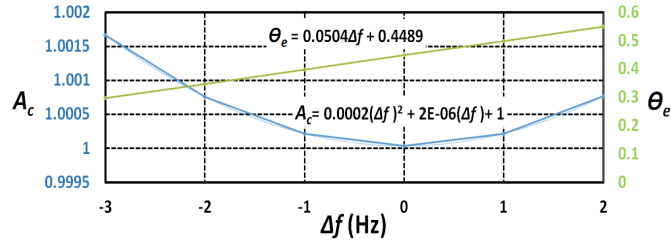
Fig. 7. Amplitude and the phase correction factor plot with regard to Δf_g

amplitude is,

$$\hat{A}_{fac} = A_c A_r \quad (27)$$

From (27), it is ensured that $\hat{A}_{fac}$ is correct estimate of A_{act}. Thus, with this approach $\hat{A}_{fac}$ can achieve adaptability to the grid frequency in a feed-forward manner.

B. Phase angle estimation and error compensation

The unit orthogonal FPS components (i.e. $|\hat{v}_\alpha^{1+}(n)|$ and $|\hat{v}_\beta^{1+}(n)|$) are utilized to estimate the phase angle information as shown below:

$$\hat{\theta} = \arctan\left[\frac{|\hat{v}_\beta^{1+}|}{|\hat{v}_\alpha^{1+}|}\right] \quad (28)$$

The errors in $\hat{\theta}$ are denoted by θ_e which is expressed as,

$$\theta_e = \theta_{ref} - \hat{\theta} \quad (29)$$

where, θ_{ref} is an artificial reference phase which is generated internally. Thereafter, θ_e is noted for every step increment in the supply frequency (i.e. from 47-52 Hz), as shown in Table II. Thus, once Δf_g is known from (21) and the curve fitting from Fig. 7, θ_e is computed as,

$$\theta_e = 0.0504(\Delta f_g) + 0.4489 \quad (30)$$

Thus, θ_e may compensate the errors present in $\hat{\theta}$ in order to estimate the actual phase angle ($\hat{\theta}_{fac}$) as follows:

$$\hat{\theta}_{fac} = \hat{\theta} + \theta_e \quad (31)$$

If $\hat{\theta}$ is ideally compensated, then it is to be understood that $\hat{\theta}_{fac}$ will be equivalent to θ_{ref}. For this purpose, phase error is presented in the simulation mode which is demonstrated after estimating $\hat{\theta}_{fac}$ and subtracting it from θ_{ref}. Further, the control parameters of the proposed algorithm are summarized in Table III.

TABLE III
CONTROL PARAMETERS FOR THE PROPOSED SCHEME

Parameters	Values
L	30
MAF pre-filter window length ($T_w = T_n/2 + T_n/6$)	13.33 ms
Fundamental period (T_n)	20 ms
DSC operator time delay ($\tau/7$)	2.86 ms
K_1, at 50 Hz	0.0078329
Sampling frequency, $f_s = 1/T_s$	12 kHz
ω_n	$2\pi50$ rad/sec
Saturation block (S_1)	3 Hz (upper limit) -4 Hz (lower limit)
Saturation block (S_2)	2 Hz (upper limit) -3 Hz (lower limit)

V. SIMULATION AND EXPERIMENTAL RESULTS

The proposed algorithm is developed in MATLAB/ Simulink environment through a discrete time solver with a fixed time step. A hardware-in-loop (HIL) simulation mode is considered for early testing of the simulated algorithm using a dSPACE DS1104 controller and an input/output CLP1104 board. The results are captured through a 16 channel DL750 scopecorder, as shown in Fig. 8. The HIL simulation-mode
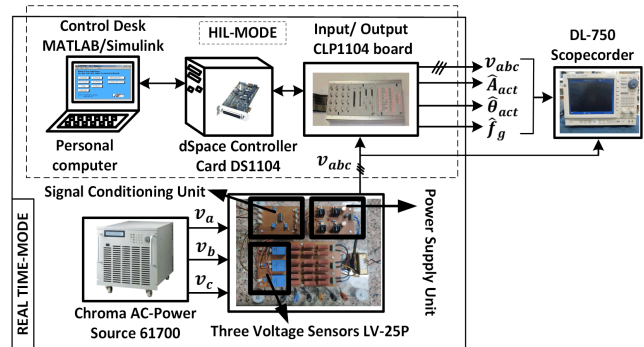
Fig. 8. Illustration of real-time simulation and its hardware setup for experimental study

(HIL-M), allows to virtually validate the complied code by internal generation of individual test input which may be uploaded to the controller card. In real time-mode (RT-M), the validation of the proposed scheme is performed by emulating the actual grid conditions through an AC-programmable power source (Chroma 61701). Herein, the controller card will only consist of the complied algorithm and the test inputs are generated from Chroma 61701. Thereafter, a compatible stepped down $\pm$ 12 V grid signal is obtained from LEM LV25-P voltage sensors. The signal conditioning unit based on operational amplifiers will receive the stepped down signal and provides a per unit (p.u.) equivalent of the grid signal. Later, the analog-to-digital converter (ADC) ports of CLP1104 input/output board will send the p.u. grid signal to the controller card for processing. The estimated parameters are obtained from the digital-to-analog converter (DAC) ports and are captured using a scopecorder. In all test cases (i.e. $A - E$) the grid voltage signal is sampled at f_s = 12 kHz while considering

each 5% of the 5th and the 7th harmonics in the grid signal for performance evaluation of the proposed scheme.

A. Phase jump and harmonics

In this test case, a 30° phase jump is considered in the grid voltage waveform at nominal frequency depicted in Fig. 9. The
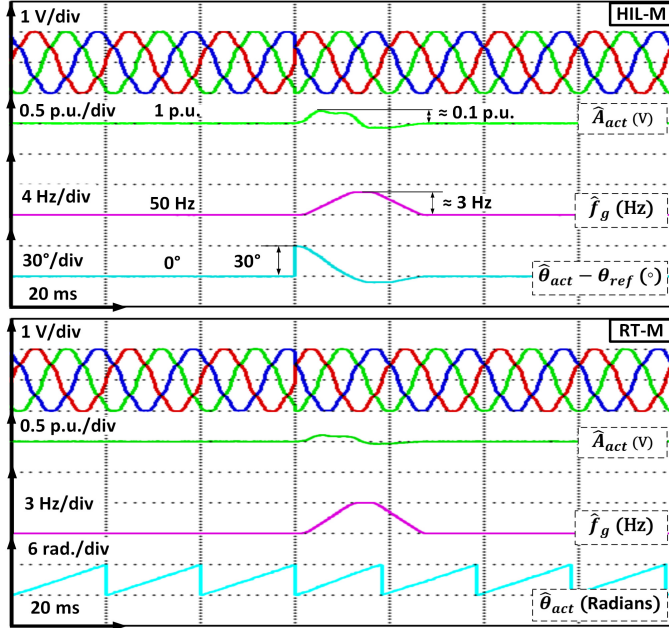

Fig. 9. In presence of harmonics the grid voltage signal is subjected to a phase jump of 30°

respective waveforms for estimated parameters are highlighted in Fig. 9. It is evident that the phase jump may be accurately estimated within 28 ms without any steady-state error. The reason for this transient duration is the reaction time taken by HPFS to extract FPS, computation of frequency deviation and the $T_w/2$ of MAF employed in the path of $\Delta \hat{f}_g$ with 16 ms, 2 ms, and 10 ms, respectively. The peak overshoot in the amplitude and the frequency is noticed as 0.1 p.u. and 3 Hz, respectively.

B. Voltage sag and harmonics

In the present study, a symmetrical voltage dip is realized by sudden reduction in nominal voltage (1 p.u.) in all phases (i.e. a-b-c) to 0.5 p.u. in both HIL-M and RT-M. In Fig. 10, it could be seen that the voltage sag is accurately tracked within 28 ms. However, frequency information will suffer from an overshoot of 2.5 Hz whereas, phase information is affected by an undershoot of −20°. Thus, the proposed scheme has a good ability to accurately track the voltage sag without involving in any steady-state oscillations.

C. Unequal DC-offset, phase jump, FNS, and harmonics

An unsymmetrical fault condition known as line-to-ground (LG) fault is tested when phase 'a' undergoes a sag of 0.1 p.u while other phases (i.e. b and c) remains at nominal value shown in Fig. 11. Thus, in grid signal there exist a 0.3 p.u. FNS component. In addition, a 30° phase jump and
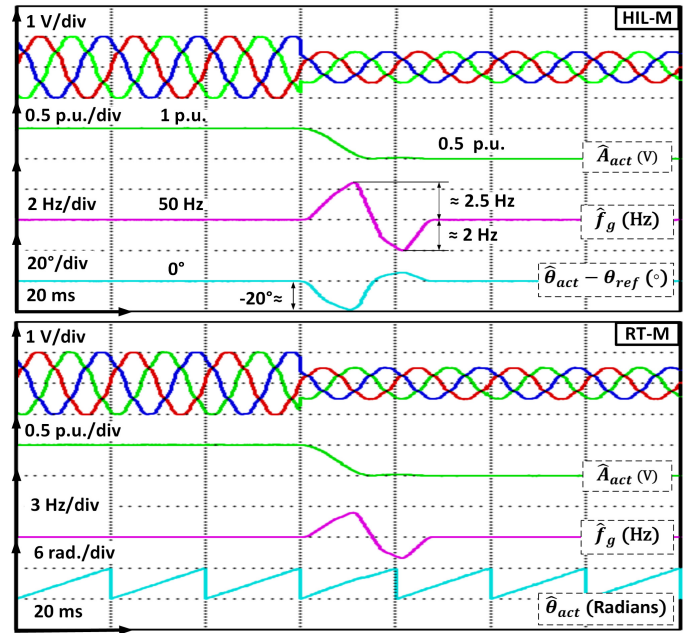

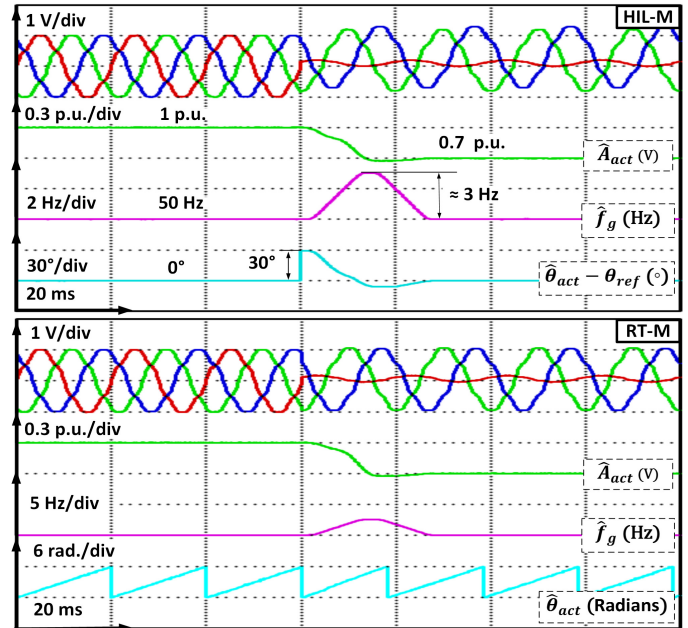Fig. 10. Symmertical grid voltage sag of 50% and harmonics

Fig. 11. Grid voltage signal contamined with harmonics, unequal DC-offset, and 0.3 p.u. of FNS including a phase jump of 30°

unequal dc offset of 0.1 p.u. (phase a), 0.2 p.u. (phase b), and 0.3 (phase c) p.u. are considered in both HIL-M and RT-M. The disturbance considered in phase and amplitude affects the frequency information with an overshoot of 3 Hz. However, the amplitude and the phase are accurately estimated within 28 ms without any steady-state error. Thus, HPFS is said to be immune towards the negative effect of DC-offset, harmonics, and FNS component.

D. FNS and frequency step

In this test, the grid voltage with 0.2 p.u. FNS and a step change of 2 Hz is considered, as shown in Fig. 12. A
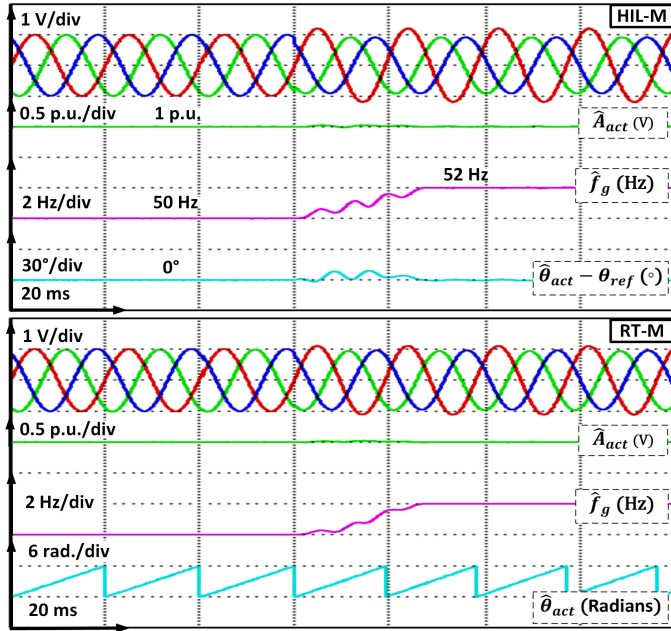

Fig. 12. Input supply frequency undergoes a step change of 2 Hz along with a 0.2 p.u. FNS in the grid signal

good immunity towards FNS is observable in the estimated parameters. Moreover, the fundamental frequency is estimated within 27 ms without significant overshoot. However, the estimation of parameters may suffer from negligible amount of steady-state oscillations in amplitude, phase, and frequency i.e. 0.003 V, 0.2°, and 0.01 Hz, respectively. The proposed scheme has the potential of frequency tracking under off-nominal frequency condition.

E. Unified test cases

Two worst test cases are presented for nominal and off-nominal frequency conditions. The grid voltage parameters are as follows: v_{abc}: 1 p.u. to 0.5 p.u., θ_{abc}: 0° to 30°, and unequal DC-offset: V_{ao}= 0.1 p.u., V_{bo}= 0.2 p.u., and V_{co}= 0.3 p.u.

1) Nominal frequency condition 50 Hz: The waveforms are presented in Fig. 13. The proposed scheme may accurately tracks the change in amplitude and phase within 28 ms without any steady-state errors. However, frequency is affected by a peak overshoot of 3 Hz.

2) Off-nominal frequency condition 47-52 Hz: From the waveforms depicted in Fig. 14. The amplitude and phase are detected within 15 ms. Since, Δf_g tends to increase from −3 Hz towards positive direction, the S_2 block will hit the saturation (i.e. 2 Hz) approximately within 15 ms. Thereby, the correct estimate of frequency is obtained within 28 ms with an overshoot of 1 Hz. The steady-state ripples in amplitude, phase, and frequency are below 0.0004 V, 0.009°, and 0.0012 Hz, respectively.
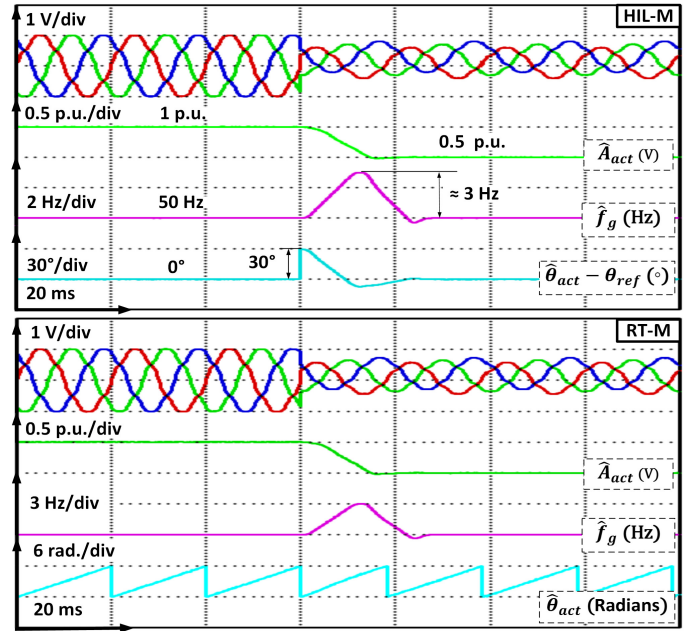

Fig. 13. Unified test case (50 Hz): the combined disturbances i.e. 50% voltage sag, 30° phase jump, and unequal DC-offset in presence of harmonics
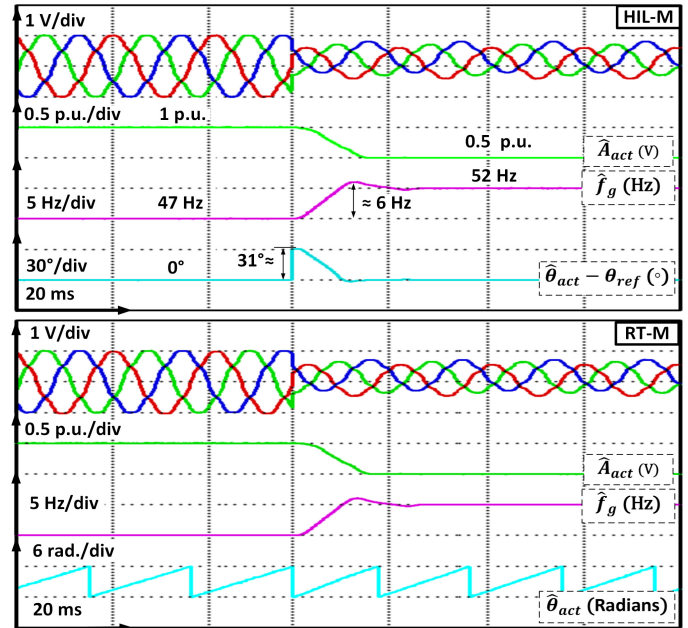
Fig. 14. Unified test case (47–52 Hz): the combined disturbances i.e. 50% voltage sag, 30° phase jump, unequal DC-offset, and harmonics

F. Comparison with various grid synchronization schemes

The performance of the proposed scheme is compared with vital schemes such as enhanced three-consecutive samples (E3CS) technique [32] developed for a single-phase application originated from generic three-phase open-loop scheme [21], multiple delayed signal cancellation–enhanced PLL (MDSC-EPLL) [9], second-order-generalized-integrator (SOGI)–FLL [8], and all-pass filter (APF)–PLL [19]. Table

IV, presents the performance of the proposed scheme vis-á-vis other techniques reported in the literature. In general, the

TABLE IV
PERFORMANCE COMPARISON OF THE PROPOSED SCHEME WITH OTHER THREE-PHASE SCHEMES

Case	Peak Errors and Settling Time	E3CS [32]	MDSC-EPLL [9]	SOGI-FLL [8]	APF-PLL [19]	Proposed Scheme
Voltage sag	δA_m (p.u.)	–	–	–	–	–
	δf_m (Hz)	NA	-0.2	1.7	0.1	2.5
	$\delta \theta_m$ (°)	NA	-2.86	-11	-0.9	-20
	t_s (ms)	20	35	40	30	28
Phase jump	δA_m (p.u.)	NA	-0.07	0.1	0.04	0.1
	δf_m (Hz)	6	8	8	2.52	3
	$\delta \theta_m$ (°)	–	0.2	–	–	–
	t_s (ms)	31	35	40	47.3	28
Frequency step	δA_m (p.u.)	-	-0.14	0.02	0.004	0.001
	δf_m (Hz)	-	-2.5	-	-	-
	$\delta \theta_m$ (°)	2.5	-0.03	5	4.5	0.2
	t_s (ms)	31	35	40	35	27
Harmonic, FNS, and DC-offset rejection		Yes	Yes	No	Yes	Yes
Steady-state frequency oscillations		Large	Medium	Large	Large	Least

proposed scheme demonstrates an improvement in response time i.e. 28 ms. It is expected that disturbance considered in the phase information affects frequency information albeit only 3 Hz overshoot is observable which is small if compared to the performance demonstrated by E3CS, MDSC–EPLL, and SOGI–FLL. Moreover, the sag induced in the grid voltage is also traced within fastest possible duration as compared to MDSC–EPLL, APF–PLL, and SOGI–FLL. In

Fig. 15. Comparison of the MAF based open-loop schemes with the proposed scheme

Fig. 15, two MAF-OSG based schemes i.e. improved open-loop synchronization technique (OLST) [33] and E3CS are compared with the proposed scheme at nominal frequency

condition where grid signal undergoes a 50% voltage sag with a combination of 30° phase jump and unequal DC-offset. It can be observed that the improved OLST, the E3CS scheme, and the proposed scheme can accurately tracks the amplitude change within 20 ms, 30 ms and 28 ms, respectively. However, due to the presence of the DC-offset in the grid signal the improved OLST suffer from oscillations in the estimated frequency and the phase information. Moreover, the proposed technique posses good ability to provide ripple free phase angle information within 28 ms. Thus, the proposed scheme demonstrates an improvement in response time by 2 ms in comparison to the E3CS technique. In Fig. 16, for an off-nominal frequency step of 2 Hz from 50 Hz in presence of harmonics, it can be observed that the steady ripples in
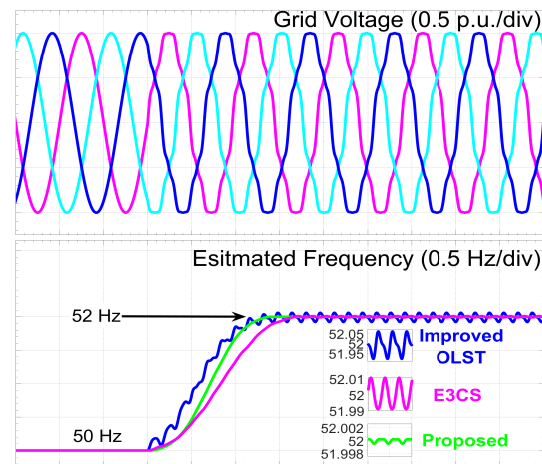

Fig. 16. Frequency step (50-52 Hz) in presence of the harmonics

the estimate of the frequency is well below the permissible limits as per the IEC standard 61000-4-7 when compared to the improved OLST and E3CS techniques.

VI. CONCLUSIONS

A non-adaptive improved digital signal processing algorithm has been reported for rapid detection of three-phase grid voltage parameters. The HPFS with ISC method ensures good rejection of DC-offset, harmonics, and FNS component under nominal and off-nominal frequency conditions. A novel fundamental frequency estimator is proposed which is based on the storage of two consecutive samples of the FPS components. The suggested modified pre-filtering unit enables to improve the overall transient response time of the scheme. Unlike PLL based schemes rigorous tuning processes are not required due to the open-loop architecture. As the feedback-loops are avoided, the real-time implementation complexity is noticed to be reduced and will not suffer from stability related issues. The fundamental grid voltage attributes are accurately estimated within 1.4 times of fundamental period. Moreover, the proposed scheme has good immunity towards grid voltage unbalance and frequency drifts. From the experimental and simulation observations, it may be inferred that the proposed feedback-less scheme is a potential choice for three-phase grid voltage monitoring, induction heating, uninterruptible power supplies, low-voltage ride through capability, etc.
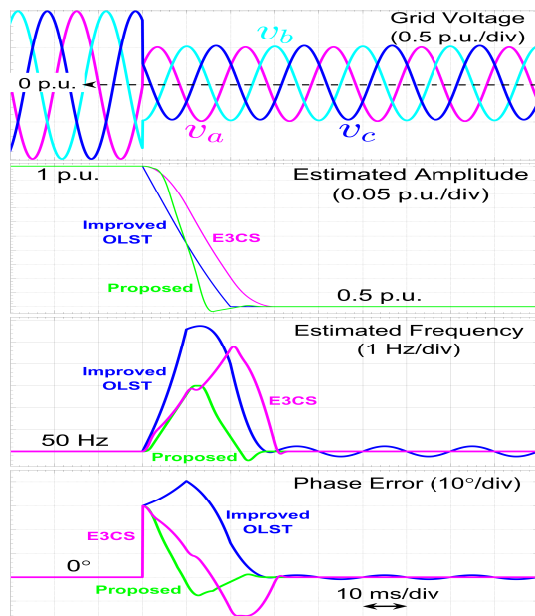
REFERENCES

[1] F. Chishti, S. Murshid, B. Singh, "Development of wind and solar based AC microgrid with power quality improvement for local non-linear load using MLMS," *IEEE Trans. Ind. Appl.*, Early Access, Jun. 2019.

[2] G. G. Talapur, H. M. Suryawanshi, L. Xu, and A. B. Shitole, "A reliable microgrid with seamless transition between grid connected and islanded mode for residential community with enhanced power quality," *IEEE Trans. Ind. Appl.*, vol. 54, no. 5, pp. 5246–5255, Sep./Oct. 2018.

[3] S. Kumar, B. Singh, "Linear coefficient function based control approach for single stage SPV system integrated to three phase distribution system," *IET Gener. Trans. Distrib.*, vol. 11, no. 3, pp. 676–684, Feb. 2017.

[4] S. Kumar, B. Singh, "Seamless operation and control of single-phase hybrid PV-BES-utility synchronized system," *IEEE Trans. Ind. Appl.*, vol. 55, no. 2, pp. 1072–1082, Mar./Apr. 2019.

[5] F. K. de A. Limaa, R. G. Araújoa, F. L. Tofolib, and C. G. C. Brancoa, "A three-phase phase-locked loop algorithm with immunity to distorted signals employing an adaptive filter," *Elect. Power Syst. Res.*, vol. 170, pp. 116–127, May 2019.

[6] Y. Bai, X. Guo, B. Wang, and Y. Li, "Fully digital grid synchronization under harmonics and unbalanced conditions," *IEEE Access*, vol. 7, pp. 109969–109981, Aug. 2019.

[7] F. Chishti, S. Murshid, B. Singh, "Weak grid intertie WEGS with hybrid generalized integrator for power quality improvement," *IEEE Trans. Ind. Electron.*, vol. 67, no. 2, pp. 1113–1123, Feb. 2020.

[8] S. Golestan, J. M. Guerrero, J. C. Vasquez, A. M. Abusorrah and Y. Al-Turki, "Modeling, tuning, and performance comparison of second-order-generalized-integrator-based FLLs," *IEEE Trans. Power Electron.*, vol. 33, no. 12, pp. 10229–10239, Dec. 2018.

[9] S. Gude and C.-C. Chu, "Dynamic performance improvement of multiple delayed signal cancelation filters based three-phase enhanced-PLL," *IEEE Trans. Ind. Appl.*, vol. 54, no. 5, pp. 5293–5305, Sep./Oct. 2018.

[10] C. I. Chen, G. W. Chang, R. C. Hong, and H. M. Li, "Extended real model of Kalman filter for time-varying harmonics estimation," *IEEE Trans. Power Del.*, vol. 25, no. 1, pp. 17–26, Jan. 2010.

[11] H. Wu, and X. Wang, "Design-oriented transient stability analysis of PLL-synchronized voltage-source converters," *IEEE Trans. Power Electron.*, Early Access, Aug. 2019.

[12] Y. Han, M. Luo, X. Zhao, J. M. Guerrero, and L. Xu, "Comparative performance evaluation of orthogonal-signal-generators-based single-phase PLL algorithms-A survey," *IEEE Trans. Power Electron.*, vol. 31, no. 5, pp. 3932–3944, May 2016.

[13] P. R.-Sánchez, X. D. T. García, A. P. Torres, and V. Feliu, "Fundamental positive- and negative-sequence estimator for grid synchronization under highly disturbed operating conditions," *IEEE Trans. Power Electron.*, vol. 28, no. 8, pp. 3733–3746, Aug. 2013.

[14] W. V. Lyon, *The Transient Analysis of Alternating-Current Machinery*. New York, NY, USA: Wiley, 1954.

[15] A. Kulkarni, and V. John, "Analysis of bandwidth?unit-vector-distortion tradeoff in PLL during abnormal grid conditions," *IEEE Trans. Ind. Electron.*, vol. 60, no. 12, pp. 5820–5829, Dec. 2013.

[16] T. Hao, F. Gao, and T. Xu, "Fast extraction of symmetrical components from distorted three-phase signals based on asynchronous-rotational reference frame," *Journ. of Power Electron.*, vol. 19, no. 4, pp. 1045–1053, Jul. 2019.

[17] J. Wang, J. Liang, F. Gao, L. Zhang, and Z. Wang, "A method to improve the dynamic performance of moving average filter-based PLL," *IEEE Trans. Power Electron.*, vol. 30, no. 10, pp. 5978–5990, Oct. 2015.

[18] D. S. S. Andrade, Y. N. Batista, F. A. S. Neves, H. E. P. de Souza, "Fast phase angle jump estimation to improve the convergence time of the GDSC-PLL," *IEEE Trans. Ind. Electron.*, Early Access, May 2019.

[19] S. Golestan, J. M. Guerrero, J. C. Vasquez, A. M. Abusorrah, and Y. Al-Turki, "All-pass-filter-based PLL systems: linear modeling, analysis, and comparative evaluation," *IEEE Trans. Power Electron.*, Early Access, Aug. 2019.

[20] X. Quan, X. Dou, Z. Wu, M. Hu, and A. Q. Huang, "Complex-coefficient complex-variable filter for grid synchronization based on linear quadratic regulation," *IEEE Trans. Ind. Informat.*, vol. 14, no. 5, pp. 1824–1834, May 2018.

[21] F. D. Freijedo, J. D.-Gandoy, Ó. López, and E. Acha, "A generic open-loop algorithm for three-phase grid voltage/current synchronization with particular reference to phase, frequency, and amplitude estimation," *IEEE Trans. Power Electron.*, vol. 24, no. 1, pp. 94–107, Jan. 2009.

[22] C. A. G. Marques, M. V. Ribeiro, and E. A. B. Da Silva, "Enhanced demodulation-based technique for estimating the parameters of fundamental component in power systems," *IET Gener. Transm. Distrib.*, vol. 5, no. 9, pp. 979–988, Sep. 2011.

[23] C. A. G. Marques, M. V. Ribeiro, C. A. Duque, P. F. Ribeiro, and E. A. B. Da Silva, "A controlled filtering method for estimating harmonics of off-nominal frequencies," *IEEE Trans. Smart Grid*, vol. 3, no. 1, pp. 38–49, Mar. 2012.

[24] M. Mirhosseini, J. Pou, V. G. Agelidis, E. Robles, and S. Ceballos, "A three-phase frequency-adaptive phase-locked loop for independent single-phase operation," *IEEE Trans. Power Electron.*, vol. 29, no. 12, pp. 6255–6259, Dec. 2014.

[25] M. S. Reza, M. Ciobotaru, and V. G. Agelidis, "A modified demodulation technique for single-phase grid voltage fundamental parameter estimation," *IEEE Trans. Ind. Electron.*, vol. 62, no. 6, pp. 3705–3713, Jun. 2015.

[26] S. Golestan, and J. M. Guerrero, "An analysis of modified demodulation-based grid voltage parameter estimator," *IEEE Trans. Power Electron.*, vol. 30, no. 12, pp. 6528–6533, Dec. 2015.

[27] K. Mathuria, I. Hussain, B. Singh, and N. Kumar, "A quadrature oscillator-based DT for accurate estimation of fundamental load current for PV system in distribution network," *IEEE Trans. Ind. Informat.*, vol. 15, no. 6, pp. 3324–3333, Jun. 2019.

[28] M. S. Reza, and V. G. Agelidis, "A demodulation-based technique for robust estimation of single-phase grid voltage fundamental parameters," *IEEE Trans. Ind. Informat.*, vol. 13, no. 1, pp. 166–175, Feb. 2017.

[29] H.-E. Liao, "Two discrete oscillator based adaptive notch filters (OS-CANFs) for noisy sinusoids," *IEEE Trans. Signal Process.*, vol. 53, no. 2, pp. 528-538, Feb. 2005.

[30] P. R.-Sánchez, X. D. T. García, A. P. Torres, and V. Feliu, "Robust frequency-estimation method for distorted and imbalanced three-phase systems using discrete filters," *IEEE Trans. Power Electron.*, vol. 26, no. 4, pp. 1089-1101, Apr. 2011.

[31] S. Reza, M. Ciobotaru, and V. G. Agelidis, "Robust frequency estimation technique based on three consecutive samples for single-phase systems," *IEEE J. Emerg. Select. Topics Power Electron.*, vol. 2, no. 4, pp. 1415-1424, Dec. 2014.

[32] S. Golestan, J. M. Guerrero, and J. C. Vasquez, "An open-loop grid synchronization approach for single-phase application," *IEEE Trans. Power Electron.*, vol. 33, no. 7, pp. 5548-5555, Jul. 2018.

[33] Peng Liu, and Shanxu Duan, "An open-loop synchronization technique with simple structure for phase error compensation and frequency estimation," *IEEE Trans. on Ind. Electron.*, Early Access, 2019.

[34] *Voltage Characteristics of Electricity Supplied by Public Distribution Systems*, Eur. Std. EN 50160, 2008.

[35] *Testing and Measurement Techniques-General Guide on Harmonics and Interharmonics Measurements and Instrumentation, for Power Supply Systems and Equipment Connected Thereto*, IEC Standard 61000-4-7, 2002.

Anant Kumar Verma (S'16-M'19) obtained his bachelor degree in Instrumentation Engineering from University Science Instrumentation Center Srinagar, India in 2012. He obtained his master's degree from Dehradun Institute of Technology (DIT), Dehradun, India in 2014. He is currently pursuing the Ph.D. degree in Electrical Engineering from National Institute of Technology, Hamirpur.

His research interests include renewable energy systems, modeling of grid synchronization algorithms, and control of power electronic converters.

Raj Kumar Jarial (M'15). He is a member of DEIS. He received his Bachelor's degree [B. Sc. Engg. (Electrical)], and Master's degree (Power System) in 1989 and 1992 respectively from the National Institute of Technology, Kurukshetra, India. Since 1994, he has been with the depart- ment of Electrical Engineering, NIT Hamirpur India. Presently, he is also the coordinator for the power transformer diagnostics center at NIT, Hamirpur, India. His current research interest includes Power Electronics based drives and High Voltage Engineering.

Pedro Roncero-Sánchez (M'07-SM'14) re- ceived an M.Sc. degree in electrical engineer- ing from Universidad Pontificia Comillas, Madrid, Spain, in 1998, and a Ph.D. degree from the University of Castilla-La Mancha, Ciudad Real, Spain, in 2004. He is currently an Associate Professor at the School of Industrial Engineer- ing, University of Castilla-La Mancha. His re- search interests include control of power elec- tronic converters, power quality, renewable en- ergy systems, energy storage devices and wire- less power transfer.

U. Mohan Rao (S'15) obtained his bachelor degree in Electrical and Electronics Engineering from Jawaharlal Nehru Technological University Kakinada, India in 2010. He obtained his mas- ter's and doctoral degrees from National Institute of Technology (NIT), Hamirpur, India in 2012 and 2017 respectively. Presently, he is a post- doctoral fellow at the Université du Québec á Chicoutimi (UQAC), Quebec, Canada with the Research Chair on the Aging of Power Network Infrastructure (ViAHT). He is a member of the IEEE DEIS and IEEE SA. Dr. Mohan is also a member of the IEEE DEIS Technical Committee on "Liquid Dielectrics" and CIGRE Canada. His main research interests include aging phenomena of high-voltage insulation, conditioning monitoring of electrical equipment, power trans- former diagnostics, and alternative liquid dielectrics.

Josep M. Guerrero (S'01-M'04-SM'08-FM'15) received the B.S. degree in telecommunications engineering, the M.S. degree in electronics engi- neering, and the Ph.D. degree in power electron- ics from the Technical University of Catalonia, Barcelona, in 1997, 2000 and 2003, respectively. Since 2011, he has been a Full Professor with the Department of Energy Technology, Aalborg University, Denmark, where he is responsible for the Microgrid Research Program. From 2014 he is chair Professor in Shandong University; from 2015 he is a distinguished guest Professor in Hunan University; and from 2016 he is a visiting professor fellow at Aston University, UK, and a guest Professor at the Nanjing University of Posts and Telecommu- nications. From 2019, he became a Villum Investigator by The Villum Fonden, which supports the Center for Research on Microgrids (CROM) at Aalborg University, being Prof. Guerrero the founder and Director of the same centre (www.crom.et.aau.dk). His research interests is oriented to different microgrid aspects, including power electronics, dis- tributed energy-storage systems, hierarchical and cooperative control, energy management systems, smart metering and the internet of things for AC/DC microgrid clusters and islanded minigrids. Specially focused on microgrid technologies applied to offshore wind and maritime micro- grids for electrical ships, vessels, ferries and seaports. Prof. Guerrero is an Associate Editor for a number of IEEE TRANSACTIONS. He has published more than 500 journal papers in the fields of microgrids and renewable energy systems, which are cited more than 40,000 times. He received the best paper award of the IEEE Transactions on Energy Conversion for the period 2014-2015, and the best paper prize of IEEE- PES in 2015. As well, he received the best paper award of the Journal of Power Electronics in 2016. During six consecutive years, from 2014 to 2019, he was awarded by Clarivate Analytics (former Thomson Reuters) as Highly Cited Researcher. In 2015 he was elevated as IEEE Fellow for his contributions on "distributed power systems and microgrids."